Original Article
Sotorasib inhibits ubiquitination degradation of TXNIP and suppresses glucose metabolism in *KRAS*[G12C] mutant bladder cancer

Zhi-Rong Zhang[1,2*], Min-Qi Liu[1,2*], Yang Ji[1,2], Di Xiao[1,2], Wei-Fan Wang[1,2], Xiao-Chen Zhou[1,2], Ling-Hui Wang[1,2], Duo Li[1,2], Hui Zou[1,2], Xiao-Ping Yang[1,2]

[1]Department of Oncology, Hunan Provincial People's Hospital, The First Affiliated Hospital of Hunan Normal University, Changsha, Hunan, China; [2]Key Laboratory of Study and Discovery of Small Targeted Molecules of Hunan Province, Engineering Research Center of Reproduction and Translational Medicine of Hunan Province, Key Laboratory of Chemical Biology and Traditional Chinese Medicine Research of Ministry of Education, Key Laboratory of Protein Chemistry and Developmental Biology of Fish of Ministry of Education, Department of Pharmacy, School of Medicine, Hunan Normal University, Changsha, Hunan, China. *Equal contributors.

Abstract: Bladder cancer is the most common malignant tumor of the urinary system. Currently, treatment strategies for bladder cancer remain limited, highlighting the urgent need to explore novel therapeutic approaches. Sotorasib, the first successful small molecule drug targeting KRAS, has been approved for treating non-small cell lung cancer (NSCLC), but it has not yet been studied in bladder cancer. Additionally, glucose metabolism-related proteins, such as GLUT1, PKM2, and LDHA are highly expressed in most bladder cancer cell lines, promoting tumor progression. *KRAS*[G12D] mutant cells exhibit enhanced glucose uptake and glycolysis. However, little is known about whether *KRAS*[G12C] mutant cells exhibit enhanced glucose metabolism. Various techniques, including glucose and lactate analysis, Seahorse assay, western blot, qRT-PCR, and immunofluorescence, were used to investigate whether Sotorasib can inhibit glucose metabolism in bladder cancer cells. The results demonstrated that Sotorasib significantly inhibited glucose metabolism in *KRAS*[G12C] mutant bladder cancer, both *in vitro* and *in vivo*, but not in wild-type bladder cancer. Furthermore, Sotorasib's inhibition of glucose metabolism was associated with suppressing the degradation of thioredoxin-interacting protein (TXNIP), a negative regulator of glucose metabolism. Additionally, Sotorasib increased TXNIP expression by regulating the RAS/RAF/ERK axis. This study uncovers the mechanism by which Sotorasib inhibits glucose metabolism in *KRAS*[G12C] mutant bladder cancer cells and suggests a potential therapeutic benefit for the treatment of *KRAS*[G12C] mutant bladder cancer.

Keywords: Bladder cancer, Sotorasib, *KRAS*[G12C] mutation, glucose metabolism, TXNIP

Introduction

Bladder cancer is the most common malignant tumor of the urinary system, ranking first in incidence among urinary system tumors in China and second to prostate cancer in Western countries. The number of new bladder cancer cases is increasing globally [1, 2]. Therefore, exploring novel therapeutic approaches is urgently needed. The Warburg effect is characteristic of both non-muscle-invasive bladder cancer (NMIBC) and muscle-invasive bladder cancer (MIBC). Studies have shown that glucose metabolism-related proteins, such as

LDHA and GLUT1, are highly expressed in most bladder cancer cell lines, promoting tumor progression [3, 4]. Additionally, the high expression of PKM2 facilitates bladder cancer growth and maintenance [5]. However, few therapeutic strategies are currently available to inhibit glucose metabolism in bladder cancer.

KRAS mutations occur with a certain frequency in bladder cancer, with the *KRAS*[G12C] mutation detected in urothelial carcinoma in situ [6, 7]. *KRAS* mutations primarily occur at codon 12 in bladder cancer [8, 9]. These mutations act as carcinogenic drivers [6, 10]; alterations in KRAS

proteins impede their interaction with GTPase-activating proteins (GAPs) and the hydrolysis of GTP bound to KRAS, leaving the protein in a constitutively active state [11, 12]. Activated KRAS can trigger multiple signaling pathways, including RAF-MEK-ERK and PI3K-AKT-mTOR pathways [13, 14]. *KRAS* mutations also impact immune cells in the tumor microenvironment (TME), ultimately contributing to tumor progression and immune evasion [15]. Some studies have shown that *KRAS* mutant pancreatic and lung cancer cells, such as those with the *KRAS*[G12D] mutation, exhibit enhanced glucose uptake and glycolysis, with GLUT1 upregulated in these cells [16, 17]. Therefore, KRAS represents a potential target for suppressing glucose metabolism. However, little is known about whether *KRAS*[G12C] mutant cells also exhibit enhanced glucose metabolism. The tumor suppressor TXNIP can promote the internalization of the glucose transporter GLUT1 and mediate the inhibition of GLUT1 mRNA and protein expression, thus regulating glucose metabolism in tumors [18-20]. Therefore, we will investigate whether TXNIP plays a role in this process.

Sotorasib, a KRAS G12C inhibitor, was approved for marketing by the FDA in 2021, marking a significant breakthrough in cancer treatment since RAS had long been considered an undruggable target. Sotorasib traps KRAS G12C in its inactive state, specifically and irreversibly inhibiting KRAS G12C [21]. In mechanistic studies, researchers found that Sotorasib inhibited the MAPK and PI3K-AKT-mTOR signaling pathways and reduced the expression of p-S6 in *KRAS*[G12C] mutant non-small cell lung cancer and pancreatic cancer cells, while increasing the expression of the apoptosis-related protein caspase-3 [22, 23]. Currently, Sotorasib is used in clinical settings for the treatment of locally advanced or metastatic non-small cell lung cancer patients with *KRAS*[G12C] mutations [24, 25]. However, it has not yet been utilized for the treatment of bladder cancer. In summary, we will explore whether Sotorasib can be applied to treat bladder cancer and inhibit glucose metabolism in this context.

Materials and methods

Cell culture

Human bladder cancer cells were obtained from iCell Bioscience Inc. (Shanghai, China). UMUC3 were cultivated in MEM (Gibco, Grand Island, NY) supplemented with 10% FBS (Excell Bio, China) and 1% penicillin/streptomycin in an incubator at 37°C with 5% CO_2. T24 were cultivated in 5A (iCell, Shanghai, China) with the same supplements.

MTT assay

Cells were plated in 96-well plates at a density of 6.0×10^3 cells per well. After 12 h, the cells were either treated with Sotorasib or FDP (fructose-1,6-diphosphate) or left untreated for 24, 48, or 72 h. Subsequently, 50 µL of MTT solution (2 mg/mL, Sigma-Aldrich, St. Louis, MO) was added to each well and incubated for 5 h. Finally, 150 µL of dimethyl sulfoxide (DMSO) was added, and the absorbance was measured at 490 nm using a microplate reader (BioTek, SYNERGY HTX, VT, USA).

Clonogenic assay

For a different assay, cells were plated in 24-well plates at a density of 2.0×10^3 cells per well. After 12 h, the cells were either treated with Sotorasib or FDP or left untreated and incubated for 5 to 7 days. Following incubation, 10% paraformaldehyde solution was added to fix the cells, and then 0.1% crystal violet was used to stain them. Absorbance was measured at 550 nm using a microplate reader (BioTek, SYNERGY HTX, VT, USA), and images of the cells were captured.

Western blot

Protein samples were resolved by SDS-PAGE and transferred to PVDF membranes, where they were probed with primary antibodies. Peroxidase-conjugated anti-rabbit or anti-mouse antibodies were used as secondary antibodies, and the antigen-antibody reactions were visualized using the ChemiDoc system (Bio-Rad, Hercules, CA, USA). The antibodies used are detailed in the Supplementary Table 1. The blot intensities were quantified using ImageJ, and the data were normalized to the loading control with an antibody against β-actin.

Immunoprecipitation

Briefly, 1.0×10^7 cells in a bottle were collected and lysed using a non-denaturing lysis buffer (Solarbio, Beijing, China). After a 30-min incu-

bation on ice, the lysate was centrifuged, and the supernatant was collected. The supernatant was then blocked with protein A/G (Santa Cruz, Dallas, TX) for 1 h. Following another centrifugation, antibodies or normal IgG were added to the supernatant and incubated overnight at 4°C. Protein A/G was added again to bind the antibody and incubated for 1 h. Protein A/G was then collected by centrifugation and washed four times with lysis buffer. A sample loading buffer (2 ×) was mixed with the beads and boiled for 10 min. The supernatant was used for western blot analysis.

Glucose analysis

Cells were plated in 6-well plates (2.5×10^5 cells/well). After 48 h, the cell culture medium was replaced with DMEM (Gibco, Grand Island, NY) supplemented with 10% FBS (Excell Bio, China) and 1% penicillin/streptomycin. After 2 h, the supernatant and cell lysate were collected. Cells were counted before being lysed with lysis buffer (Beyotime, Shanghai, China). In the remaining wells, cells were treated or not treated with Sotorasib. After 24 h, the supernatant and cell lysate were collected. Then, 10 μL of the samples were mixed with 180 μL of glucose assay reagent (Beyotime, Shanghai, China). The mixture was heated at 95°C for 8 min using a high-capacity cDNA reverse transcription kit (Thermo, Shanghai, China). A total of 150 μL of the reaction mixture was added to 96-well plates. Absorbance was measured at 630 nm using a microplate reader (BioTek, SYNERGY HTX, VT, USA). The concentration of glucose in the samples was calculated based on a standard curve.

Lactate analysis

Cells were plated in 6-well plates at a density of 2.5×10^5 cells per well. After 48 h, the cell culture medium was replaced with DMEM (Gibco, Grand Island, NY) supplemented with 10% FBS (Excell Bio, China) and 1% penicillin/streptomycin. The supernatant and cell lysate were collected after 2 h. Cells were counted before being lysed with lysis buffer (Beyotime, Shanghai, China). In the remaining wells, cells were either treated or not treated with Sotorasib. After 24 h, the supernatant and cell lysate were collected again. Subsequently, 5-μL samples were transferred into 96-well plates. Each reagent from the lactate assay kit

(Elabscience, Wuhan, China) was added sequentially. Absorbance was measured at 530 nm using a microplate reader (BioTek, SYNERGY HTX, VT, USA). Lactate concentration in the samples was calculated based on a standard curve.

qRT-PCR

RNA was extracted using Trizol reagent. Complementary DNA (cDNA) was synthesized using a high-capacity cDNA reverse transcription kit (Thermo, Shanghai, China). Quantitative RT-PCR (qRT-PCR) was performed using TaqMan Gene Expression Master Mix (Bio-Rad, Shanghai, China). The sequences of the primers are provided in the Supplementary Table 2.

siRNA transfection

Cells were plated in 6-well plates at a density of 2.5×10^5 cells per well. After 12 h, cells were transfected with 25 nM RNAi oligonucleotides and 25 nM Negative Control siRNA (Ribobio, Shanghai, China) using Lipofectamine 6000 (Invitrogen, Eugene, USA) in the absence of FBS for 5 h. Subsequently, cells were washed with PBS, and the medium was replaced with MEM for 24 h. Proteins were then collected, and specific silencing was confirmed by western blot. The sequences of the siRNAs are provided in the Supplementary Table 3.

Immunofluorescence

Briefly, 1.0×10^4 cells were seeded on glass coverslips. Cells were either treated or not treated with Sotorasib, then washed three times with PBS and fixed with 4% paraformaldehyde for 30 min. After another washing step, cells were incubated for 30 min with 4% BSA. Cells were incubated overnight at 4°C with the primary antibody. Following two PBS washes, DyLight 549-labeled secondary antibody (Proteintech, Chicago, USA) was added and incubated for 1 h. Nuclei were stained with DAPI and fixed in glycerin before being imaged using a fluorescence microscope. Fluorescence intensities were quantified using ImageJ and normalized to the loading control.

Measurement of extracellular fluxes

Cells were analyzed for glycolytic and mitochondrial function using Seahorse XF24 (Agilent,

Santa Clara, CA, USA) equipped with Glycolysis Stress Test Kit (103020-100) and Mito Stress Test Kit (103015-100). Following Sotorasib treatment, 2.5×10^4 cells were seeded in an XF24 well cell culture microplate and incubated overnight at 37°C under 5% CO_2. Four corner wells were filled with medium for background correction. To assess oxidative respiration, the medium was replaced with 500 μL of Seahorse XF DMEM (103575-100) containing 1 mM pyruvate (103578-100), 2 mM glutamine (103579-100), and 10 mM glucose (103577-100). For glycolytic activity, 500 μL of Seahorse XF DMEM (103575-100) devoid of glucose and pyruvate was used, followed by a 1-h incubation at 37°C in a CO_2-free environment. Oxygen consumption rate (OCR) and extracellular acidification rate (ECAR) were quantified using the XF24 Extracellular Flux Analyzer. ECAR measurements were performed first without additives, followed by sequential addition of glucose (10 mM), oligomycin (1 μM), and 2-DG (50 mM). OCR measurements were conducted after baseline assessments with subsequent addition of oligomycin (1.5 μM), FCCP (1 μM), and rotenone/antimycin A (0.5 μM).

Subcutaneous xenograft model study

Female BALB/c nude mice, aged 4 to 6 weeks (n=40), were procured from GemPharmatech LLC (Jiangsu, China). The study was sanctioned by the Ethics Committee of Hunan Normal University (D2023001). Mice were randomized into groups and subcutaneously injected with UMUC3 or T24 cell suspensions to create xenograft models. Tumor volumes were measured using the formula: $1/2 \times$ long diameter $\times$ short diameter^2. Treatment commenced when tumors reached 50 mm^3, with mice receiving either Sotorasib or vehicle (0.5% carboxy methyl cellulose sodium) through gavage. Tumor volumes and body weights were recorded every 2 days. Following 14 days of treatment, the mice were euthanized, and their livers and kidneys were paraffin-embedded, sectioned, and histologically examined. All tumors were preserved in formalin for subsequent Ki-67 and WB analysis. The investigators were blinded to group assignments during the evaluation of the results.

Histology

Tissues were fixed with 4% paraformaldehyde for 24 h, embedded in paraffin, and sectioned to a thickness of 7 μm. Sections were stained with hematoxylin and eosin (H&E) and evaluated for disease presence. For immunohistochemistry staining, sections were deparaffinized and rehydrated sequentially in xylene, 100%, 95%, and 75% ethanol. They were then incubated with 3% H_2O_2 for 20 min to inhibit endogenous peroxidase activity, rinsed with PBS, and subjected to antigen retrieval in Tris-EDTA solution for 5 min in a pressure cooker. Overnight incubation at 4°C followed, using the primary antibody anti-Ki-67. After additional washes in PBS, sections were treated with Reagent 2 and Reagent 3 from the Goat Hypersensitivity Two-Step Detection Kit (ZSGB-BIO, Beijing, China), as per the manufacturer's instructions. Staining was completed using a DAB substrate kit (Cell Signaling, Beverly, MA, USA) and counterstaining with Gill's hematoxylin (Solarbio, Beijing, China). Finally, sections were dehydrated and mounted with neutral resins (Solarbio, China). IHC staining analysis data were quantified using Image J and normalized to the load control.

UALCAN database analysis

The relationship between the expression of glucose metabolism-related genes and the survival of bladder cancer patients was examined using the UALCAN database. TCGA database was selected and gene names were entered. Then the specific cancer type was chosen before generating the survival curves.

Statistical analysis

Data from three independent experiments were presented as mean ± SD. Statistical analyses were conducted using Graphpad Prism 6. Two-tailed unpaired Student t-tests and one-way analysis of variance (ANOVA) were applied. Variances between groups were also statistically compared. All experiments were conducted at least three times. A *p*-value of less than 0.05 was considered statistically significant.

Results

The survival of bladder cancer patients is negatively correlated with the expression levels of SLC2A1 (GLUT1) and PKM2

Firstly, we explored the relationship between the expression of *SLC2A1* and *PKM2* and the

A

Effect of SLC2A1 expression level on BLCA patient survival

p = 0.0082

B

Effect of PKM2 expression level on BLCA patient survival

p = 0.024
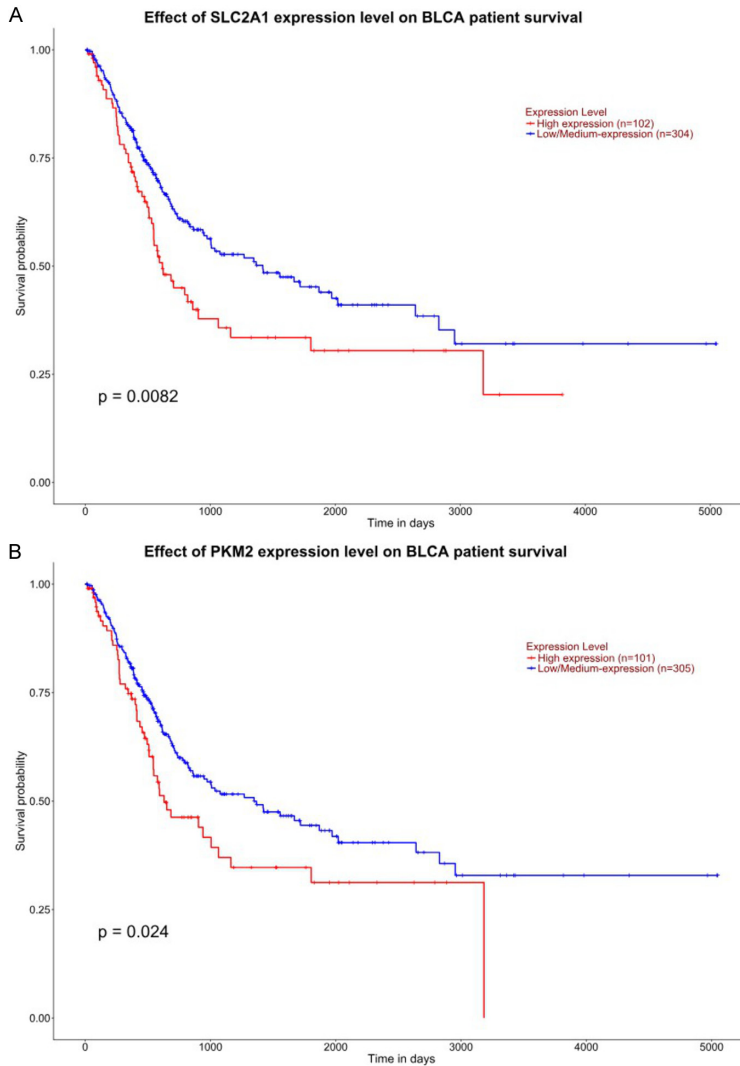
Figure 1. Relationship between the expression of *SLC2A1* and *PKM2* and patient survival. (A, B) UALCAN database was used to analyze the relationship between the patient survival and expression of *SLC2A1* and *PKM2*.

survival of bladder cancer patients using the UALCAN database [26, 27]. The results indicated that the survival of bladder cancer patients is negatively correlated with the expression levels of *SLC2A1* and *PKM2* (**Figure 1A** and **1B**).

KRAS^{G12C} mutant bladder cancer cells possess enhanced glucose metabolism capabilities and are more sensitive to Sotorasib

UMUC3 is a *KRAS^{G12C}* mutant bladder cancer cell line, while T24 is a wild-type bladder cancer cell line. We analyzed the basal levels of glucose consumption and lactate production in both UMUC3 and T24. The results demonstrated that UMUC3 exhibited higher glucose con-

sumption and lactate production levels compared to T24 (**Figure 2A** and **2B**). Additionally, western blot (WB) analysis revealed that GLUT1 expression was higher in UMUC3 than in T24 (**Figure 2C**). These findings suggested that *KRAS^{G12C}* mutant bladder cancer cells possess enhanced glucose metabolism capabilities.

To investigate the effect of the *KRAS^{G12C}* mutation on sensitivity to Sotorasib, we found that Sotorasib had a stronger inhibitory effect on the proliferation of UMUC3, as evidenced by the MTT assay. The IC$_{50}$ values for Sotorasib in UMUC3 and T24 were 35 μM and 55 μM, respectively (**Figure 2D**). Further experiments using colony formation assays confirmed that Sotorasib inhibited the proliferation of bladder cancer cells, with a more pronounced effect observed in UMUC3 (**Figure 2E**). These results indicated that *KRAS^{G12C}* mutant bladder cancer cells are more sensitive to Sotorasib.

Sotorasib inhibited glucose metabolism in KRAS^{G12C} mutant bladder cancer cells

Since *KRAS* mutations can enhance glucose uptake and glycolysis [28, 29], we speculated whether Sotorasib interferes with glucose metabolism in *KRAS^{G12C}* mutant bladder cancer cells. Following treatment with 16 μM Sotorasib, glucose consumption and lactate production in UMUC3 decreased by 24.9% and 16.6%, respectively, within 24 h. In contrast, glucose consumption and lactate production in T24 did not decrease (**Figure 3A** and **3B**). The oxygen consumption rate (OCR) results indicated a decrease following Sotorasib treatment, while the extracellular acidification rate (ECAR) also declined after treatment. These results suggested that both glycolysis and oxidative phosphorylation (OXPHOS) were inhibited after Sotorasib treatment (**Figure 3C** and **3D**). To fur-
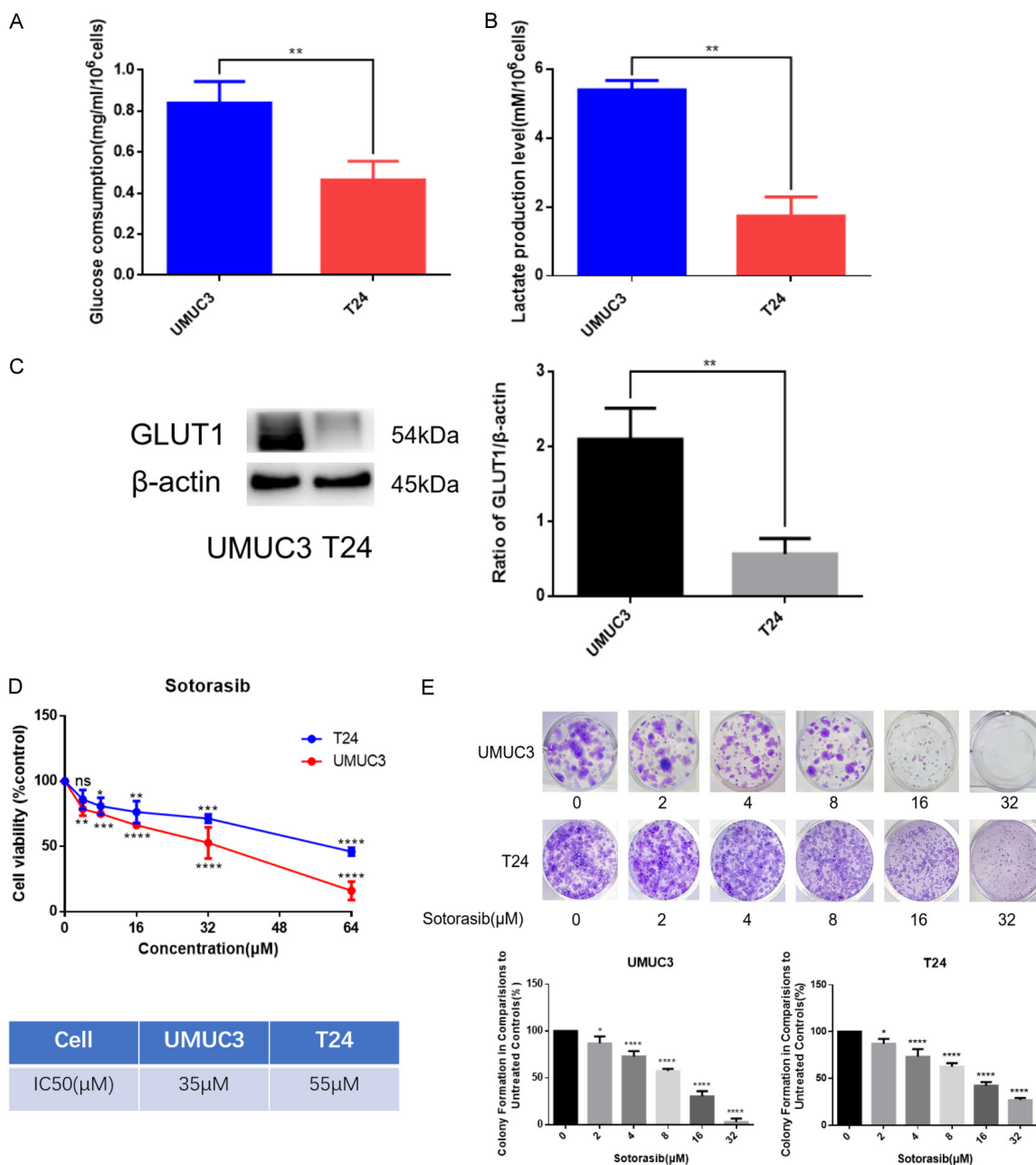
Figure 2. Comparison on the glucose metabolism and the sensitivity to Sotorasib of $KRAS^{G12C}$ mutant and wild-type bladder cancer cells. (A) When UMUC3 and T24 density reached 60%-70%, the supernatant and cell lysate were collected. Cells were counted before lysed. After 24 h, the supernatant and cell lysate were collected. Then glucose consumption was detected by glucose detection kit. (B) Steps before detection were the same as those for (A). Then lactate production was detected by lactate detection kit. (C) Expression of GLUT1 in UMUC3 and T24 was detected by WB. (D) Inhibitory effects of Sotorasib on the proliferation of UMUC3 and T24 were detected by MTT assay. IC_{50} values were counted by SPSS 20.0. (E) Inhibitory effects of Sotorasib on the proliferation of UMUC3 and T24 were detected by colony formation assay (*$P < 0.05$, **$P < 0.01$, ***$P < 0.001$, ****$P < 0.0001$, ns not significant, n=3).

ther validate these findings, we measured the mRNA levels of glucose metabolism-related proteins using qRT-PCR. The results showed that the mRNA expression of GLUT1, PKM2, and LDHA was inhibited after treatment with 16

µM and 32 µM Sotorasib in UMUC3 but not in T24 (Figure 3E). Additionally, WB analysis demonstrated that the protein expression of GLUT1, PKM2, and LDHA was similarly inhibited in UMUC3 following 16 µM and 32 µM Sotorasib
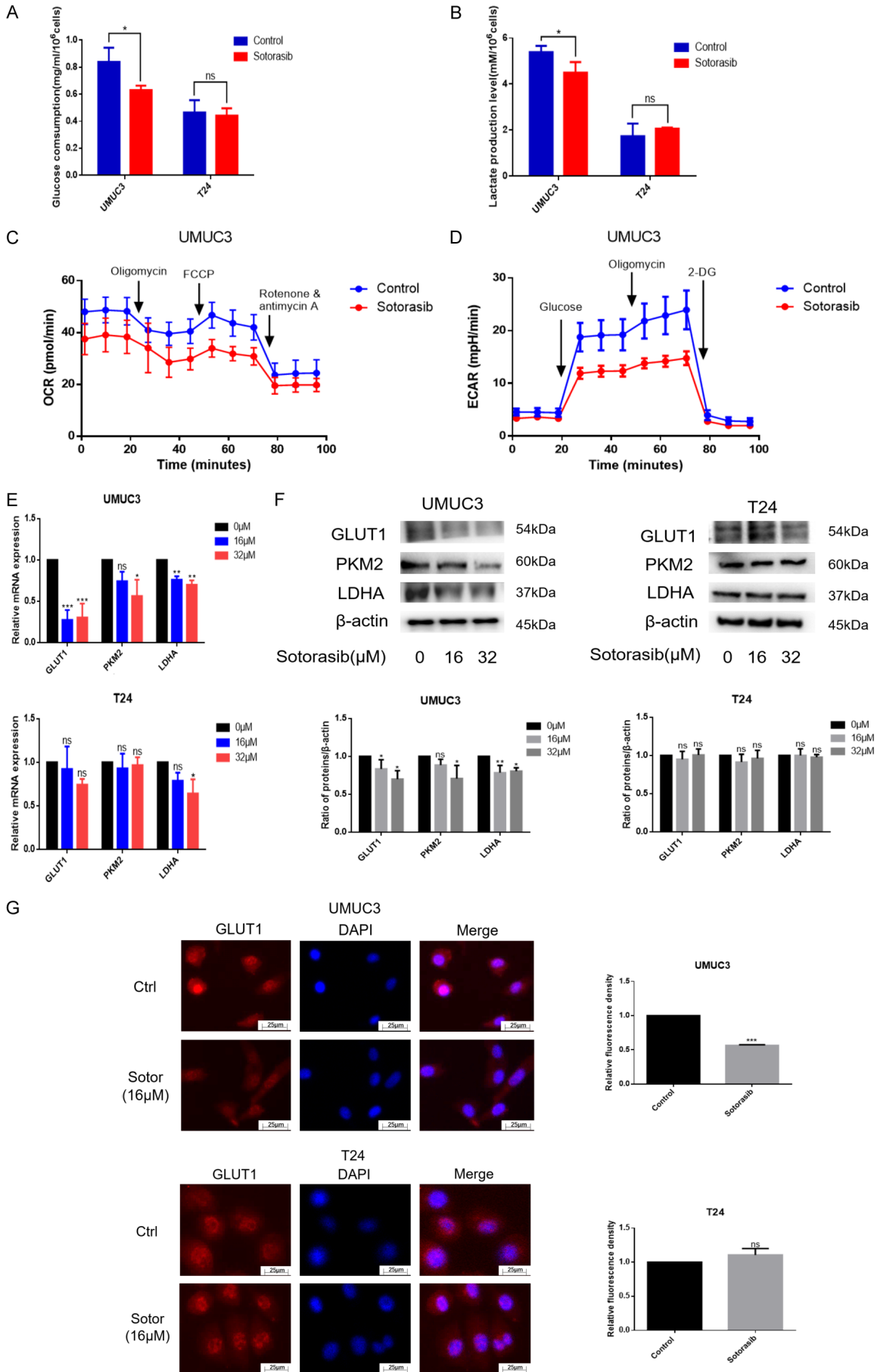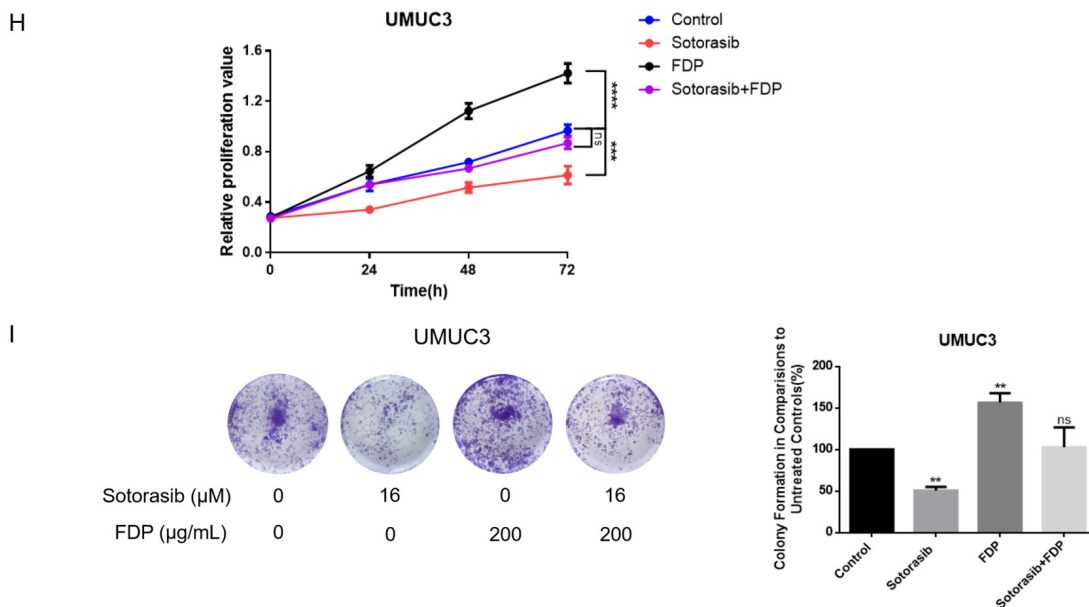
Figure 3. Impact of Sotorasib on glucose metabolism in *KRAS*^{G12C} mutant bladder cancer cells. (A) Glucose consumption was measured using a glucose detection kit. (B) The steps before detection were the same as (A), then lactate production was detected with a lactate detection kit. (C) UMUC3 with or without Sotorasib treatment (16 µM), were analyzed for oxygen consumption rate via Seahorse assay. (D) The extracellular acidification rate was examined using the same assay. (E and F) UMUC3 and T24 were treated with various concentrations of Sotorasib (0, 16, and 32 µM) for 12 h and underwent mRNA and protein expression analyses of GLUT1, PKM2, and LDHA by qRT-PCR and WB, respectively. (G) The expression of GLUT1 in treated or untreated UMUC3 and T24 was detected by immunofluorescence. (H and I) The proliferation of UMUC3 treated with Sotorasib (16 µM) or FDP (200 µg/mL) was monitored using MTT and colony formation assays, respectively (*$P < 0.05$, **$P < 0.01$, ***$P < 0.001$, ****$P < 0.0001$, ns not significant, n=3).

treatment, while no changes were observed in T24 (**Figure 3F**). Immunofluorescence results further confirmed that GLUT1 expression was inhibited in UMUC3 but not in T24 (**Figure 3G**). In conclusion, Sotorasib effectively inhibited glycolysis and OXPHOS in *KRAS*^{G12C} mutant bladder cancer cells.

To investigate the role of glucose metabolism in the effects of Sotorasib, UMUC3 were treated with FDP (fructose-1,6-diphosphate), a glycolysis agonist, alongside Sotorasib. Cell proliferation was assessed using MTT and colony formation assays. FDP, a critical intermediate in the glycolysis pathway, enhances glucose metabolism. Our findings revealed a significant increase in UMUC3 proliferation following treatment with 200 µg/mL of FDP, which nearly abolished the inhibitory effect of Sotorasib on cell growth. These results indicated that the suppression of glucose metabolism was a key mechanism by which Sotorasib inhibited the proliferation of *KRAS*^{G12C} mutant bladder cancer cells (**Figure 3H** and **3I**).

Sotorasib increased the expression of TXNIP by inhibiting its ubiquitination degradation

Initially, we observed an increase in TXNIP expression in UMUC3 but not in T24 (**Figure 4A**). To further elucidate how Sotorasib modulates TXNIP expression, we first analyzed its mRNA levels. According to **Figure 4B**, Sotorasib treatment did not significantly alter TXNIP mRNA levels in *KRAS*^{G12C} mutant bladder cancer cells, although protein levels increased following treatment. This suggested that Sotorasib may influence the post-transcriptional regulation of TXNIP. Subsequently, UMUC3 were treated with CHX (cycloheximide, a protein synthesis inhibitor) in the absence or presence of Sotorasib to explore its effect on TXNIP protein synthesis post-transcriptionally. WB results indicated that the degradation rate of TXNIP decreased following Sotorasib treatment, suggesting that Sotorasib inhibited TXNIP degradation (**Figure 4C**). To investigate the primary site of TXNIP degradation, UMUC3 were treated with cycloheximide (CHX) and subsequently
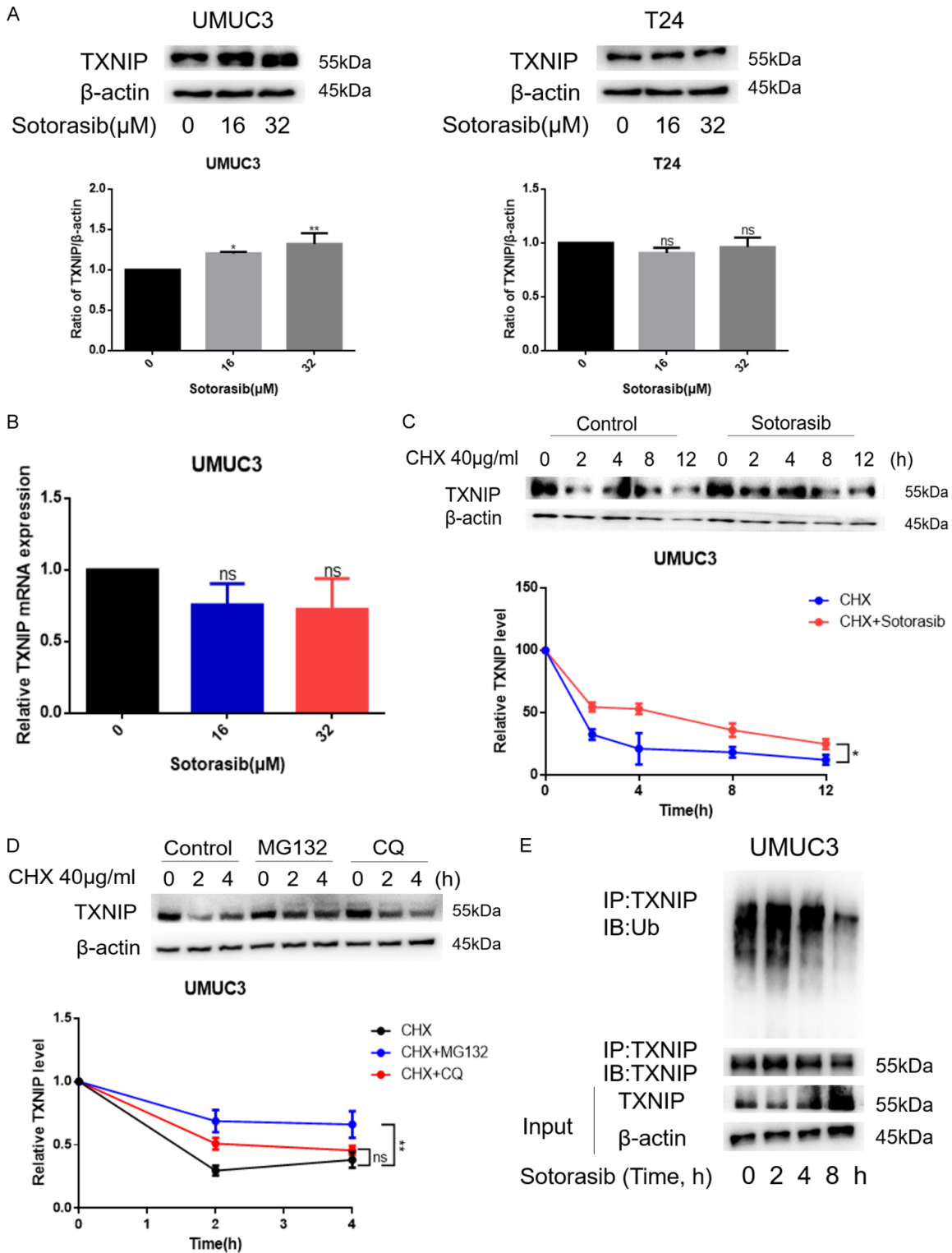
Figure 4. Effect of Sotorasib on TXNIP. (A) UMUC3 and T24 were treated with Sotorasib (0, 16, and 32 µM) for 12 h. Protein expression of TXNIP was detected by WB. (B) Steps before detection were the same as (A). mRNA expression of TXNIP was detected by qRT-PCR. (C) UMUC3 were treated with CHX (40 µg/mL; 0, 2, and 4 h) and either treated or not treated with Sotorasib (16 µM; 0, 2, and 4 h). The degradation rate of TXNIP was detected by WB. (D) UMUC3 were treated with CHX (40 µg/mL; 0, 2, and 4 h) and treated with MG132 (1 µM) or CQ (5 µM). The degradation rate of TXNIP was detected by WB. (E) UMUC3 were treated with Sotorasib (16 µM; 0 h, 2 h, 4 h, and 8 h). The protein lysates were immunoprecipitated with TXNIP antibody. The immunoprecipitates were tested by WB with antibodies to TXNIP and Ub (*$P < 0.05$, **$P < 0.01$, ***$P < 0.001$, ****$P < 0.0001$, ns not significant, n=3).

exposed to either MG132 (a proteasome inhibitor) or chloroquine (CQ, a lysosome inhibitor). The results indicated that TXNIP degradation decreased after treatment with both MG132 and CQ, with a more significant reduction observed after MG132 treatment, suggesting that the proteasome is the primary site of TXNIP degradation (**Figure 4D**). Additionally, we found that TXNIP ubiquitination was reduced after Sotorasib treatment, indicating that Sotorasib inhibited the ubiquitination degradation of TXNIP (**Figure 4E**). Thus, Sotorasib increased the expression of TXNIP by inhibiting its ubiquitination degradation.

TXNIP is a negative regulator of glucose metabolism

To explore the relationship between TXNIP and glucose metabolism, we silenced TXNIP in $KRAS^{G12C}$ mutant bladder cancer cells and observed a significant increase in glucose consumption and lactate production within 24 h (**Figure 5A** and **5B**). Investigating the underlying mechanism, we found that the mRNA expression of glucose metabolism-related proteins GLUT1, PKM2, and LDHA increased upon TXNIP silencing (**Figure 5C**). Correspondingly, WB results confirmed that the expression of these proteins also increased when TXNIP was silenced (**Figure 5D**). Immunofluorescence further validated that GLUT1 expression increased in the absence of TXNIP (**Figure 5E**). In summary, TXNIP acts as a negative regulator of glucose metabolism.

Next, we verified whether Sotorasib's inhibition of glucose metabolism is linked to TXNIP regulation. Results from glucose consumption and lactate production experiments indicated that Sotorasib's inhibition of these processes decreased when TXNIP was silenced (**Figure 5F** and **5G**). Furthermore, WB results demonstrated that the inhibition of glucose metabolism-related proteins GLUT1, PKM2, and LDHA by Sotorasib diminished when TXNIP was silenced (**Figure 5H**). These findings indicated that Sotorasib inhibited glucose metabolism in $KRAS^{G12C}$ mutant bladder cancer cells through TXNIP regulation.

Sotorasib increased TXNIP expression by modulating the RAS/RAF/ERK axis

To determine whether Sotorasib upregulated the expression of TXNIP by regulating the RAS/

RAF/ERK axis, we first assessed the effect of Sotorasib on this pathway. After RAS activation, activated RAS binds to the N-terminal domain of RAF, thereby activating the downstream MAPK pathway [30]. Notably, the binding of KRAS to cRAF in UMUC3 was stronger than in T24 (**Figure 6A**). Following treatment with 16 µM Sotorasib, the binding of KRAS to cRAF in UMUC3 decreased, while no decrease was observed in T24 (**Figure 6B**). Similarly, WB results indicated that treatment with 16 µM and 32 µM Sotorasib inhibited the expression of p-cRAF and p-ERK in UMUC3, but did not affect these proteins in T24. Furthermore, Sotorasib inhibited the expression of bypass proteins p-AKT and p-mTOR in UMUC3, while no inhibition was noted in T24 (**Figure 6C**).

To investigate the relationship between TXNIP and the RAS/RAF/ERK axis, we examined the expression changes of KRAS, cRAF, and ERK upon silencing TXNIP. WB results showed no significant changes in the expression of KRAS, cRAF, and ERK, indicating that TXNIP is located downstream of the RAS/RAF/ERK axis (**Figure 6D**). Previous research has suggested that TXNIP may prevent bladder cancer by inhibiting ERK activation [31]. Additionally, Kelleher et al. proposed that TNF-α-induced degradation of TXNIP is ERK-dependent [32]. Therefore, we speculated that the inhibition of TXNIP degradation by Sotorasib is ERK-dependent. We found that after treatment with TBHQ (tert-Butylhydroquinone, an ERK activator), ERK phosphorylation increased and TXNIP expression decreased. Conversely, after Selumetinib (an ERK inhibitor) treatment, ERK phosphorylation decreased and TXNIP expression increased, indicating that ERK phosphorylation status regulates TXNIP expression. Furthermore, we observed that the inhibition of TXNIP degradation by Sotorasib was reduced when ERK phosphorylation increased, and conversely, this inhibition increased when ERK phosphorylation decreased (**Figure 6E**). At the same time, following either inhibition or activation of ERK phosphorylation, the inhibition of TXNIP ubiquitination by Sotorasib showed a similar trend (**Figure 6F**). These results indicated that Sotorasib's inhibition of TXNIP degradation was related to ERK phosphorylation. To explore the mechanism further, we conducted co-immunoprecipitation (CO-IP) experiments. The results demonstrated that TXNIP bound to both p-ERK and ERK, with a stronger binding affinity to
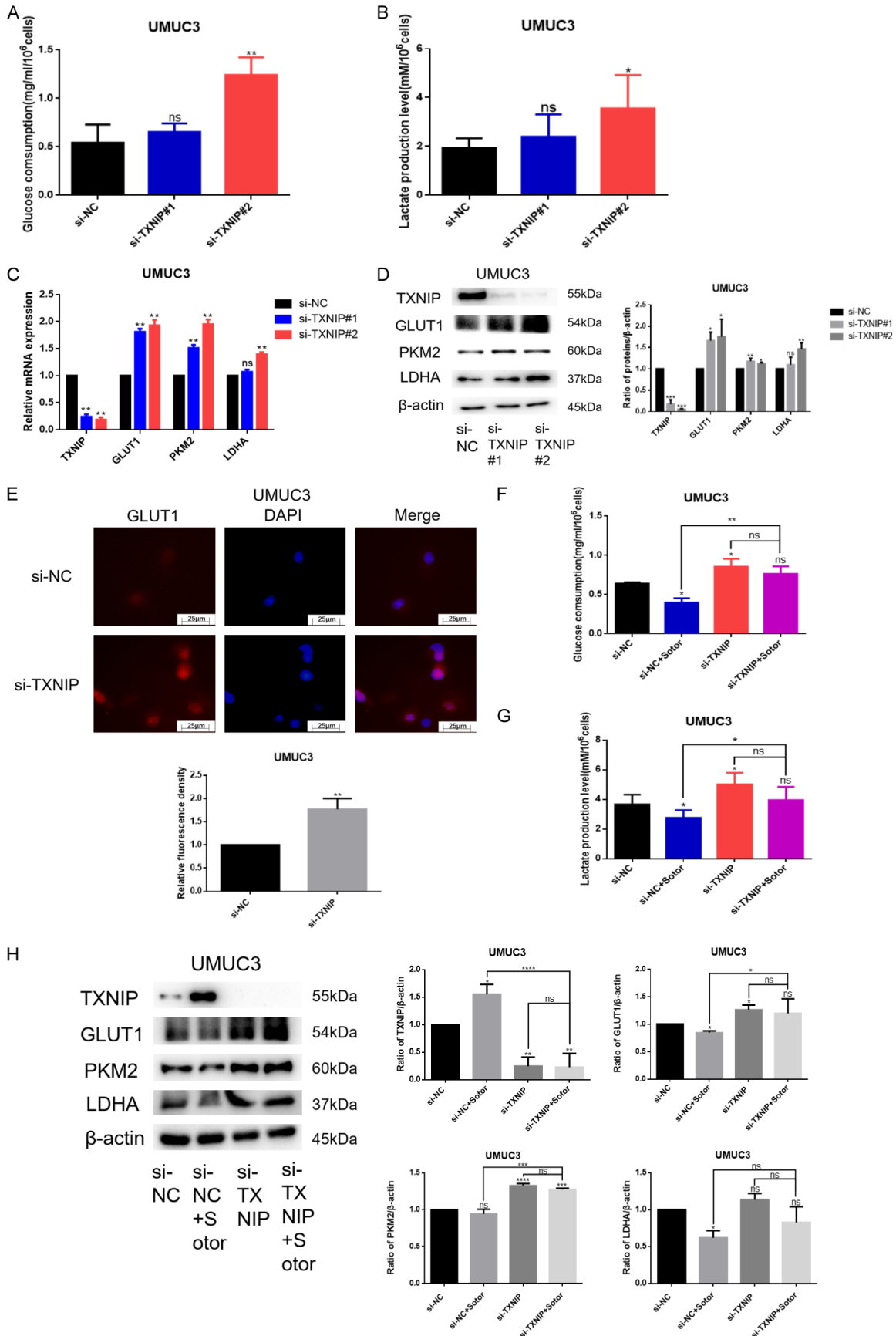
Figure 5. Effect of TXNIP on glucose metabolism in either absence or presence of Sotorasib. (A) UMUC3 were transfected by 25 nM TXNIP RNAi oligonucleotides and 25 nM negative control siRNA with the transfection reagent Lipofectamine 6000 in the absence of FBS for 5 h. UMUC3 were washed with PBS, and the medium was replaced for 24 h. Finally, glucose consumption was detected using a glucose detection kit. (B) Treatment on UMUC3 was the same as that for (A). Then lactate production was detected using a lactate detection kit. (C) UMUC3 were transfected by TXNIP RNAi oligonucleotides. And then the mRNA expression of TXNIP, GLUT1, PKM2, and LDHA was detected by qRT-PCR. (D) Treatment on UMUC3 was the same as that for (C). The protein expression of TXNIP, GLUT1, PKM2, and LDHA was detected by WB. (E) Expression of GLUT1 was detected by immunofluorescence. (F) UMUC3 were transfected by TXNIP RNAi oligonucleotides. Then UMUC3 were treated or not treated with Sotorasib (16 μM) for 12 h. Glucose consumption was detected by glucose detection kit. (G) Treatment on UMUC3 was the same as that for (F). Lactate production was detected using a lactate detection kit. (H) UMUC3 were transfected by TXNIP RNAi oligonucleotides. And then UMUC3 were treated or not treated with Sotorasib (16 μM) for 12 h. The protein expression of TXNIP, GLUT1, PKM2, and LDHA was detected by WB ($*P < 0.05$, $**P < 0.01$, $***P < 0.001$, $****P < 0.0001$, ns, not significant, n=3).
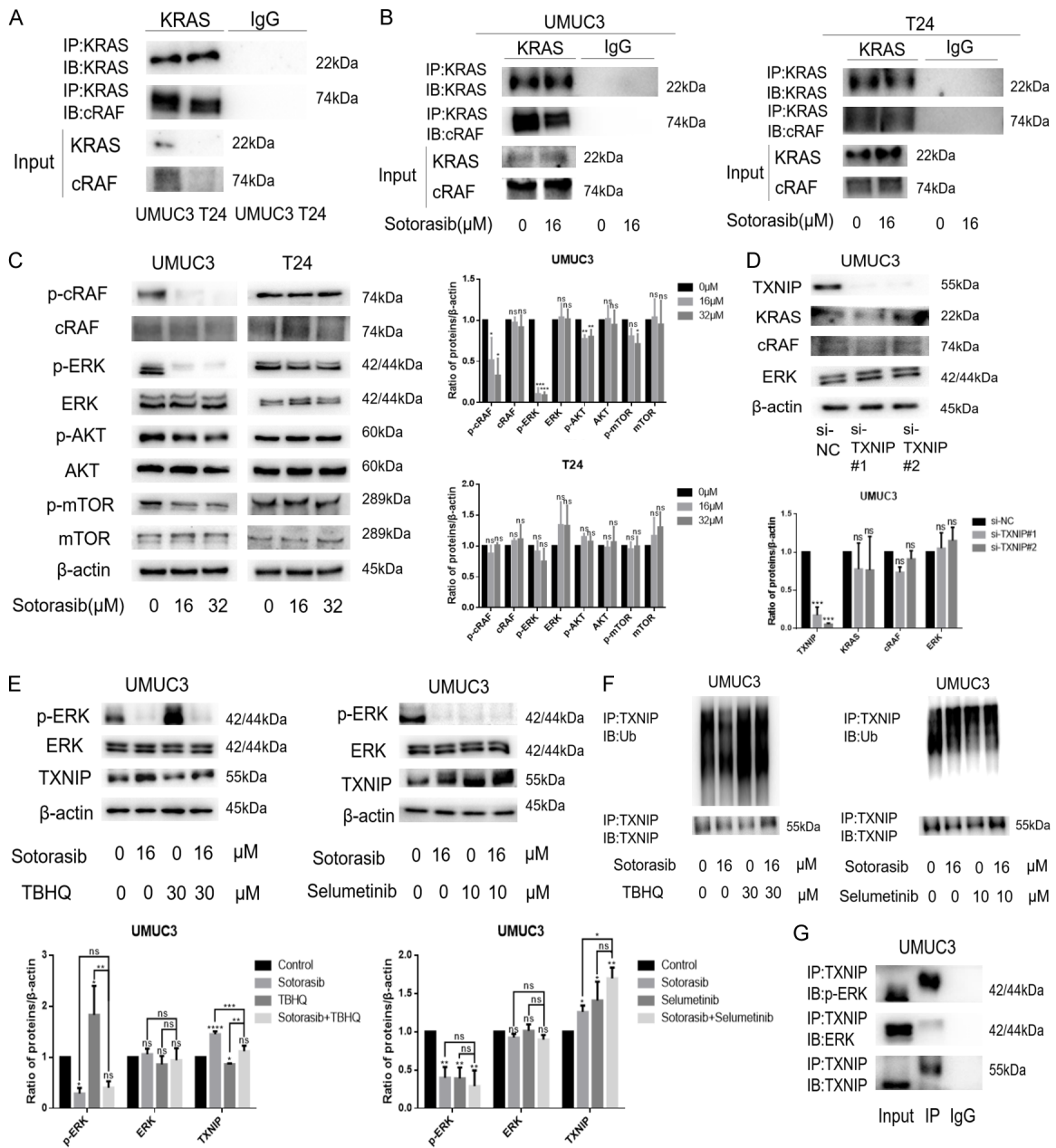
Figure 6. Effect of Sotorasib on TXNIP expression associated with the RAS/RAF/ERK axis. (A) The binding of KRAS to cRAF in UMUC3 and T24 was detected by CO-IP and WB experiments. The protein lysates were immunoprecipitated with KRAS antibody. The immunoprecipitates were tested using WB with antibodies to KRAS and cRAF. (B) UMUC3 and T24 were treated with Sotorasib for 12 h. Then the protein lysates were immunoprecipitated with KRAS antibody. The immunoprecipitates were tested by WB with antibodies to KRAS and cRAF. (C) UMUC3 and T24 were treated with Sotorasib (0 μM, 16 μM, and 32 μM) for 12 h. And the protein expression of p-cRAF, cRAF, p-ERK, ERK, p-AKT, AKT, p-mTOR, and mTOR was detected by WB. (D) UMUC3 were transfected by TXNIP RNAi oligonucleotides. The protein expression of TXNIP, KRAS, cRAF, and ERK was detected by WB. (E) UMUC3 were treated or not treated with Sotorasib (16 μM) for 12 h. At the same time, UMUC3 were treated or not treated with TBHQ (30 μM) or Selumetinib (10 μM) for 12 h. The protein expression of p-ERK, ERK, and TXNIP was detected by WB. (F) Treatment on UMUC3 was the same as that for (E), and then the protein lysates were immunoprecipitated with TXNIP antibody. The immunoprecipitates were tested by WB with antibodies to TXNIP and Ub. (G) The protein lysates were immunoprecipitated with TXNIP antibody. The immunoprecipitates were tested by WB with antibodies to TXNIP, p-ERK, and ERK (*$P < 0.05$, **$P < 0.01$, ***$P < 0.001$, ****$P < 0.0001$, ns not significant, n=3).

p-ERK and a weaker affinity to ERK. This suggested that p-ERK regulates TXNIP through direct binding (**Figure 6G**). In conclusion, Sotorasib increased TXNIP expression by modulating the RAS/RAF/ERK axis.

Sotorasib inhibited the growth of xenograft bladder tumor in vivo and the expression of glucose metabolism-related proteins in KRAS^{G12C} mutant bladder tumor

In this study, we demonstrated that Sotorasib inhibited the growth of bladder cancer cells. To further verify its effect on bladder tumor growth, we conducted *in vivo* experiments using UMUC3 and T24 xenograft models in BALB/c-Nude mice. Once the tumor volume reached 50 mm³, the mice were treated with Sotorasib (10 mg/kg) every 2 days. As shown in **Figure 7A** and **7D**, the volume of UMUC3 xenograft tumors significantly decreased following Sotorasib treatment. **Figure 7C** illustrated a corresponding reduction in the weight of UMUC3 xenograft tumors. In contrast, the volume and weight of T24 xenograft tumors decreased to a lesser extent after Sotorasib treatment. There was no significant difference in the body weight of nude mice between the treatment and control groups (**Figure 7B**). Additionally, H&E staining revealed no evident toxicity in the liver and kidneys after Sotorasib treatment, although the arrangement of tumor cells appeared more chaotic and loose in the treatment groups compared to the control groups (**Figure 7E**). Immunohistochemical analysis of Ki-67 indicated a significant reduction in the number of Ki-67-positive tumor cells in the UMUC3 group following Sotorasib treatment, whereas the decrease in the T24 group was less pronounced (**Figure 7F**). WB analysis showed that the expression of glucose metabo-lism-related proteins GLUT1, PKM2, and LDHA in UMUC3 xenograft tumors was significantly downregulated after Sotorasib treatment, while TXNIP expression was significantly upregulated. In T24 xenograft tumors, there were no significant changes in the expression of GLUT1 and TXNIP, whereas PKM2 was downregulated and LDHA was upregulated (**Figure 7G**).

Discussion

In recent years, several studies have demonstrated that the oncogene *KRAS* plays a critical role in regulating cancer metabolism by orchestrating multiple metabolic changes [33]. Additionally, some researchers have indicated that targeting the Warburg effect in *KRAS*^{G12D} glycolytic tumor organoids enhances the toxicity of 5-FU without affecting non-transformed wild-type cells [34]. On the other hand, the first KRAS inhibitor, Sotorasib, specifically targets KRAS G12C and is currently used clinically for the treatment of locally advanced or metastatic non-small cell lung cancer patients with *KRAS*^{G12C} mutation [22, 35]. However, Sotorasib has not yet been studied in bladder cancer. Therefore, we proposed the hypothesis that Sotorasib can be used to inhibit glucose metabolism in *KRAS*^{G12C} mutant bladder cancer.

Firstly, we found that bladder cancer cells with *KRAS*^{G12C} mutation demonstrated enhanced glucose metabolism capabilities. Additionally, experiments measuring glucose consumption and lactate production, along with Seahorse assays, revealed that Sotorasib impeded glucose metabolism in these cells. The mechanism behind this was linked to Sotorasib's suppression of TXNIP ubiquitination degradation. Sotorasib increased TXNIP expres-
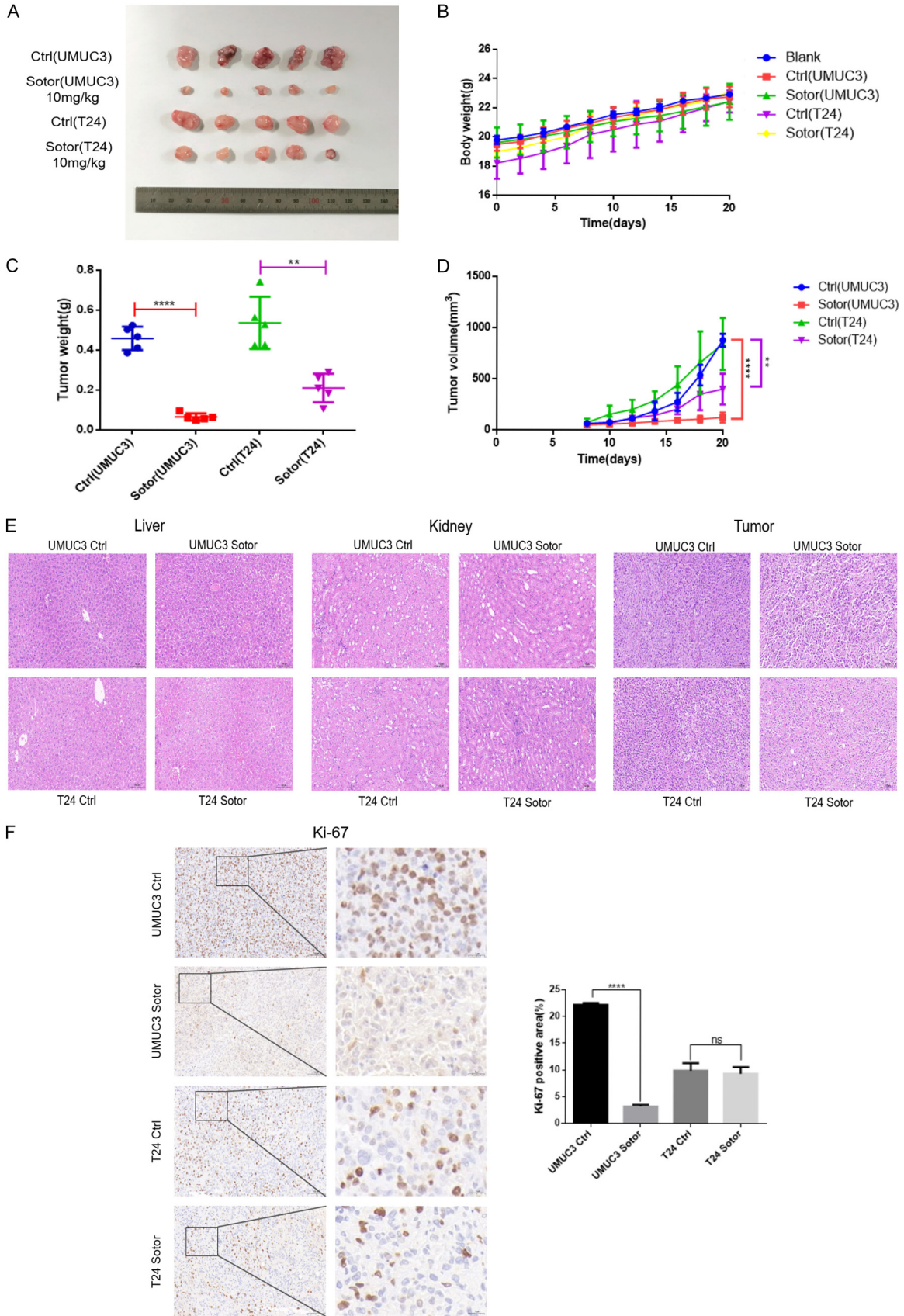
The effect of Sotorasib on bladder cancer

G
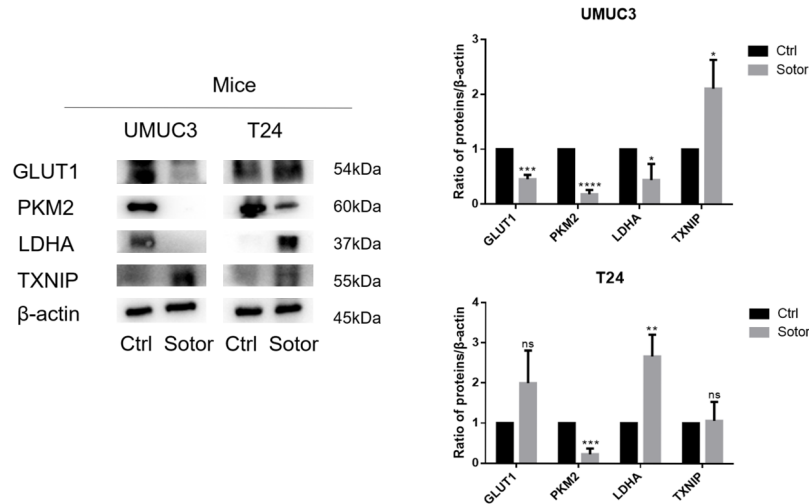
Figure 7. Inhibitory effect of Sotorasib on xenograft bladder tumor *in vivo*. (A) UMUC3 and T24 xenograft models were established in BALB/c-Nude mice. When the tumor volume reached 50 mm³, nude mice were treated with Sotorasib (10 mg/kg) every 2 days. After 14 days of Sotorasib treatment, the tumors were removed and photographed. (B) The body weights were recorded every 2 days. (C) After the tumors were removed, the tumor weights were recorded. (D) The tumor volumes were recorded every 2 days. Tumor volumes were calculated according to the formula: $1/2 \times$ long diameter $\times$ short diameter^2. (E) H&E staining of liver, kidney, and tumor. (F) Expression of Ki-67 in tumor tissues was detected by immunohistochemistry. (G) Protein expression of GLUT1, PKM2, LDHA, and TXNIP in tumor tissues was detected by WB (*$P < 0.05$, **$P < 0.01$, ***$P < 0.001$, ****$P < 0.0001$, ns not significant, n=3).
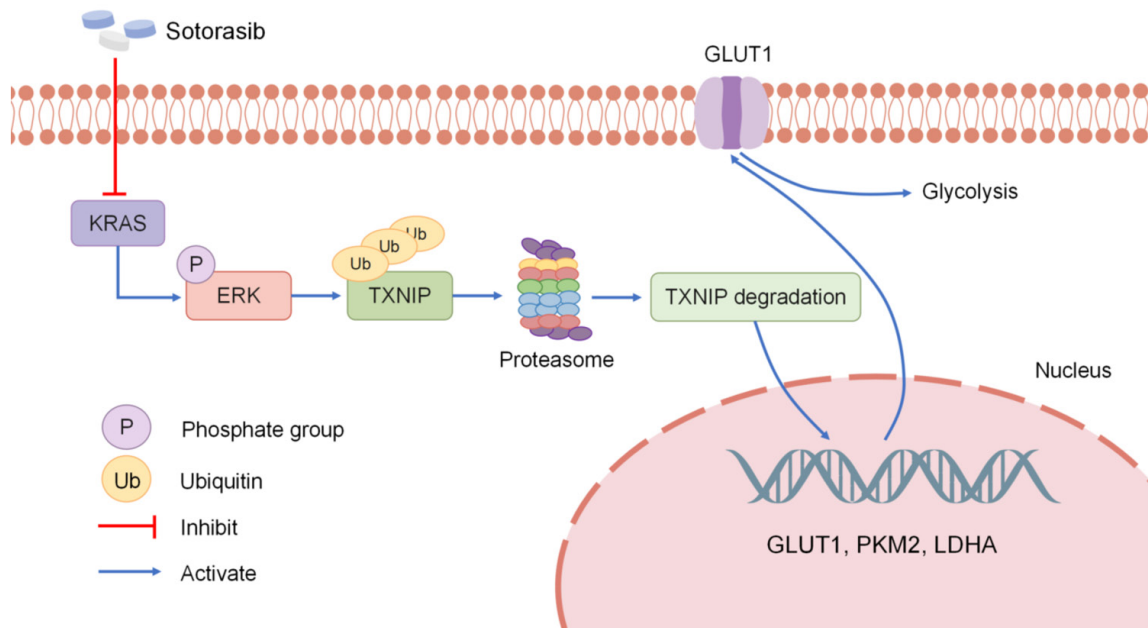
Figure 8. Summary of the mechanisms. Sotorasib specifically inhibits KRAS and then suppresses the phosphorylation of ERK; therefore, the ubiquitination of TXNIP decreases. After the ubiquitination degradation of TXNIP in the proteasome decreases, the mRNA and protein expression of GLUT1, PKM2, and LDHA is inhibited; therefore, the glucose metabolism is inhibited.

sion by modulating the RAS/RAF/ERK axis. Concurrently, we investigated Sotorasib's impact on glucose metabolism in bladder tumors through *in vivo* experiments. Results showed that Sotorasib significantly curtailed the growth of *KRAS^G12C* mutant bladder tumors and

reduced the expression of glucose metabolism-related proteins (**Figure 8**).

To date, there has been limited research on the application of Sotorasib in treating bladder cancer. Our study indicated that Sotorasib can inhibit glucose metabolism in *KRAS*^{G12C} mutant bladder cancer and delved into the mechanisms underlying this inhibition, potentially aiding the development of new bladder cancer treatments.

Our findings suggested that Sotorasib's effect on TXNIP ubiquitination is linked to ERK phosphorylation. However, specific studies on how phosphorylated ERK (p-ERK) influences TXNIP ubiquitination have not yet been conducted. Some research suggested that TXNIP's ubiquitination degradation is related to its phosphorylation [36]. Our study also discovered that p-ERK associates with TXNIP, though the specific phosphorylation sites remain unidentified. Other studies have shown that ERK-dependent TXNIP ubiquitination and proteasome degradation hinge on phosphorylation at a PXTP motif threonine (Thr349) within the C-terminal α-arrestin domain, close to a known E3 ubiquitin ligase binding site [32].

Although Sotorasib exhibits anticancer activity in preclinical studies and has demonstrated effective remission, disease stability, and absence of dose-limiting toxic effects in clinical trials, these benefits are often short-lived due to the development of resistance [37]. Resistance represents a significant challenge in the clinical use of Sotorasib, primarily due to mutations in *EGFR/FGFR*, secondary *RAS* mutations, alterations in other genes, and activation of the PI3K pathway [35, 38, 39]. To counteract resistance, combining Sotorasib with other targeted therapies is considered a viable approach to extend the duration of response or reverse drug resistance [40].

Acknowledgements

Disclosure of conflict of interest

None.

Address correspondence to: Duo Li, Hui Zou and Xiao-Ping Yang, School of Medicine, Hunan Normal University, Changsha, Hunan, China. Fax: +86-182-2975-1147; E-mail: liduo@hunnu.edu.cn (DL); Fax: +86-137-8710-8416; E-mail: zouhui@hunnu.edu.cn (HZ); Fax: +86-158-7406-6132; E-mail: xiaoping.yang@hunnu.edu.cn (XPY)

References

[1] Dobruch J and Oszczudłowski M. Bladder cancer: current challenges and future directions. Medicina (Kaunas) 2021; 57: 749.

[2] Martinez Rodriguez RH, Buisan Rueda O and Ibarz L. Bladder cancer: present and future. Med Clin (Barc) 2017; 149: 449-455.

[3] Burns JE, Hurst CD, Knowles MA, Phillips RM and Allison SJ. The Warburg effect as a therapeutic target for bladder cancers and intratumoral heterogeneity in associated molecular targets. Cancer Sci 2021; 112: 3822-3834.

[4] Afonso J, Gonçalves C, Costa M, Ferreira D, Santos L, Longatto-Filho A and Baltazar F. Glucose metabolism reprogramming in bladder cancer: Hexokinase 2 (HK2) as prognostic biomarker and target for bladder cancer therapy. Cancers (Basel) 2023; 15: 982.

[5] Xia Y, Wang X, Liu Y, Shapiro E, Lepor H, Tang MS, Sun TT and Wu XR. PKM2 is essential for bladder cancer growth and maintenance. Cancer Res 2022; 82: 571-585.

[6] Buyucek S, Coskun SK, Onal B, Gamsizkan M, Cangur S and Esbah O. Receptor tyrosine kinase pathway and infiltrating urothelial carcinoma. J Environ Pathol Toxicol Oncol 2023; 42: 65-77.

[7] Li X, Liu J, Li A, Liu X, Miao Y and Wang Z. Analysis of the relationship between bladder cancer gene mutation and clinical prognosis by high-throughput sequencing. Lab Med 2023; 54: 142-152.

[8] Ouerhani S, Bougatef K, Soltani I, Elgaaied AB, Abbes S and Menif S. The prevalence and prognostic significance of KRAS mutation in bladder cancer, chronic myeloid leukemia and colorectal cancer. Mol Biol Rep 2013; 40: 4109-4114.

[9] Ouerhani S and Elgaaied AB. The mutational spectrum of HRAS, KRAS, NRAS and FGFR3 genes in bladder cancer. Cancer Biomark 2011-2012; 10: 259-266.

[10] McDonald ER 3rd, de Weck A, Schlabach MR, Billy E, Mavrakis KJ, Hoffman GR, Belur D, Castelletti D, Frias E, Gampa K, Golji J, Kao I, Li L,

Megel P, Perkins TA, Ramadan N, Ruddy DA, Silver SJ, Sovath S, Stump M, Weber O, Widmer R, Yu J, Yu K, Yue Y, Abramowski D, Ackley E, Barrett R, Berger J, Bernard JL, Billig R, Brachmann SM, Buxton F, Caothien R, Caushi JX, Chung FS, Cortés-Cros M, deBeaumont RS, Delaunay C, Desplat A, Duong W, Dwoske DA, Eldridge RS, Farsidjani A, Feng F, Feng J, Flemming D, Forrester W, Galli GG, Gao Z, Gauter F, Gibaja V, Haas K, Hattenberger M, Hood T, Hurov KE, Jagani Z, Jenal M, Johnson JA, Jones MD, Kapoor A, Korn J, Liu J, Liu Q, Liu S, Liu Y, Loo AT, Macchi KJ, Martin T, McAllister G, Meyer A, Mollé S, Pagliarini RA, Phadke T, Repko B, Schouwey T, Shanahan F, Shen Q, Stamm C, Stephan C, Stucke VM, Tiedt R, Varadarajan M, Venkatesan K, Vitari AC, Wallroth M, Weiler J, Zhang J, Mickanin C, Myer VE, Porter JA, Lai A, Bitter H, Lees E, Keen N, Kauffmann A, Stegmeier F, Hofmann F, Schmelzle T and Sellers WR. Project DRIVE: a compendium of cancer dependencies and synthetic lethal relationships uncovered by large-scale, deep RNAi screening. Cell 2017; 170: 577-592, e510.

[11] Hunter JC, Manandhar A, Carrasco MA, Gurbani D, Gondi S and Westover KD. Biochemical and structural analysis of common cancer-associated KRAS mutations. Mol Cancer Res 2015; 13: 1325-1335.

[12] Ostrem JM and Shokat KM. Direct small-molecule inhibitors of KRAS: from structural insights to mechanism-based design. Nat Rev Drug Discov 2016; 15: 771-785.

[13] Huang L, Guo Z, Wang F and Fu L. KRAS mutation: from undruggable to druggable in cancer. Signal Transduct Target Ther 2021; 6: 386.

[14] Hoxhaj G and Manning BD. The PI3K-AKT network at the interface of oncogenic signalling and cancer metabolism. Nat Rev Cancer 2020; 20: 74-88.

[15] Dias Carvalho P, Guimarães CF, Cardoso AP, Mendonça S, Costa ÂM, Oliveira MJ and Velho S. KRAS oncogenic signaling extends beyond cancer cells to orchestrate the microenvironment. Cancer Res 2018; 78: 7-14.

[16] Yun J, Rago C, Cheong I, Pagliarini R, Angenendt P, Rajagopalan H, Schmidt K, Willson JK, Markowitz S, Zhou S, Diaz LA Jr, Velculescu VE, Lengauer C, Kinzler KW, Vogelstein B and Papadopoulos N. Glucose deprivation contributes to the development of KRAS pathway mutations in tumor cells. Science 2009; 325: 1555-1559.

[17] Kim D, Min D, Kim J, Kim MJ, Seo Y, Jung BH, Kwon SH, Ro H, Lee S, Sa JK and Lee JY. Nutlin-3a induces KRAS mutant/p53 wild type lung cancer specific methuosis-like cell death that is dependent on GFPT2. J Exp Clin Cancer Res 2023; 42: 338.

[18] Ji S, Qin Y, Liang C, Huang R, Shi S, Liu J, Jin K, Liang D, Xu W, Zhang B, Liu L, Liu C, Xu J, Ni Q, Chiao PJ, Li M and Yu X. FBW7 (F-box and WD repeat domain-containing 7) Negatively regulates glucose metabolism by targeting the c-Myc/TXNIP (thioredoxin-binding protein) axis in pancreatic cancer. Clin Cancer Res 2016; 22: 3950-3960.

[19] Dagdeviren S, Lee RT and Wu N. Physiological and pathophysiological roles of thioredoxin interacting protein: a perspective on redox inflammation and metabolism. Antioxid Redox Signal 2023; 38: 442-460.

[20] Herzig S and Shaw RJ. AMPK: guardian of metabolism and mitochondrial homeostasis. Nat Rev Mol Cell Biol 2018; 19: 121-135.

[21] Skoulidis F, Li BT, Dy GK, Price TJ, Falchook GS, Wolf J, Italiano A, Schuler M, Borghaei H, Barlesi F, Kato T, Curioni-Fontecedro A, Sacher A, Spira A, Ramalingam SS, Takahashi T, Besse B, Anderson A, Ang A, Tran Q, Mather O, Henary H, Ngarmchamnanrith G, Friberg G, Velcheti V and Govindan R. Sotorasib for lung cancers with KRAS p.G12C mutation. N Engl J Med 2021; 384: 2371-2381.

[22] Canon J, Rex K, Saiki AY, Mohr C, Cooke K, Bagal D, Gaida K, Holt T, Knutson CG, Koppada N, Lanman BA, Werner J, Rapaport AS, San Miguel T, Ortiz R, Osgood T, Sun JR, Zhu X, McCarter JD, Volak LP, Houk BE, Fakih MG, O'Neil BH, Price TJ, Falchook GS, Desai J, Kuo J, Govindan R, Hong DS, Ouyang W, Henary H, Arvedson T, Cee VJ and Lipford JR. The clinical KRAS (G12C) inhibitor AMG 510 drives anti-tumour immunity. Nature 2019; 575: 217-223.

[23] Xue JY, Zhao Y, Aronowitz J, Mai TT, Vides A, Qeriqi B, Kim D, Li C, de Stanchina E, Mazutis L, Risso D and Lito P. Rapid non-uniform adaptation to conformation-specific KRAS (G12C) inhibition. Nature 2020; 577: 421-425.

[24] Nakajima EC, Drezner N, Li X, Mishra-Kalyani PS, Liu Y, Zhao H, Bi Y, Liu J, Rahman A, Wearne E, Ojofeitimi I, Hotaki LT, Spillman D, Pazdur R, Beaver JA and Singh H. FDA approval summary: sotorasib for KRAS G12C-mutated metastatic NSCLC. Clin Cancer Res 2022; 28: 1482-1486.

[25] de Langen AJ, Johnson ML, Mazieres J, Dingemans AC, Mountzios G, Pless M, Wolf J, Schuler M, Lena H, Skoulidis F, Yoneshima Y, Kim SW, Linardou H, Novello S, van der Wekken AJ, Chen Y, Peters S, Felip E, Solomon BJ, Ramalingam SS, Dooms C, Lindsay CR, Ferreira CG, Blais N, Obiozor CC, Wang Y, Mehta B, Varrieur T, Ngarmchamnanrith G, Stollenwerk B, Waterhouse D and Paz-Ares L; CodeBreaK 200 Investigators. Sotorasib versus docetaxel for previously treated non-small-cell lung cancer with KRAS (G12C) mutation: a randomised, open-

label, phase 3 trial. Lancet 2023; 401: 733-746.

[26] Chandrashekar DS, Karthikeyan SK, Korla PK, Patel H, Shovon AR, Athar M, Netto GJ, Qin ZS, Kumar S, Manne U, Creighton CJ and Varambally S. UALCAN: an update to the integrated cancer data analysis platform. Neoplasia 2022; 25: 18-27.

[27] Chandrashekar DS, Bashel B, Balasubramanya SAH, Creighton CJ, Ponce-Rodriguez I, Chakravarthi B and Varambally S. UALCAN: a portal for facilitating tumor subgroup gene expression and survival analyses. Neoplasia 2017; 19: 649-658.

[28] Ying H, Kimmelman AC, Lyssiotis CA, Hua S, Chu GC, Fletcher-Sananikone E, Locasale JW, Son J, Zhang H, Coloff JL, Yan H, Wang W, Chen S, Viale A, Zheng H, Paik JH, Lim C, Guimaraes AR, Martin ES, Chang J, Hezel AF, Perry SR, Hu J, Gan B, Xiao Y, Asara JM, Weissleder R, Wang YA, Chin L, Cantley LC and DePinho RA. Oncogenic Kras maintains pancreatic tumors through regulation of anabolic glucose metabolism. Cell 2012; 149: 656-670.

[29] Liu YH, Hu CM, Hsu YS and Lee WH. Interplays of glucose metabolism and KRAS mutation in pancreatic ductal adenocarcinoma. Cell Death Dis 2022; 13: 817.

[30] Lu S, Jang H, Muratcioglu S, Gursoy A, Keskin O, Nussinov R and Zhang J. Ras conformational ensembles, allostery, and signaling. Chem Rev 2016; 116: 6607-6665.

[31] Chen Y, Ning J, Cao W, Wang S, Du T, Jiang J, Feng X and Zhang B. Research progress of TXNIP as a tumor suppressor gene participating in the metabolic reprogramming and oxidative stress of cancer cells in various cancers. Front Oncol 2020; 10: 568574.

[32] Kelleher ZT, Wang C, Forrester MT, Foster MW and Marshall HE. ERK-dependent proteasome degradation of Txnip regulates thioredoxin oxidoreductase activity. J Biol Chem 2019; 294: 13336-13343.

[33] Kawada K, Toda K and Sakai Y. Targeting metabolic reprogramming in KRAS-driven cancers. Int J Clin Oncol 2017; 22: 651-659.

[34] Ludikhuize MC, Gevers S, Nguyen NTB, Meerlo M, Roudbari SKS, Gulersonmez MC, Stigter ECA, Drost J, Clevers H, Burgering BMT and Rodríguez Colman MJ. Rewiring glucose metabolism improves 5-FU efficacy in p53-deficient/KRAS (G12D) glycolytic colorectal tumors. Commun Biol 2022; 5: 1159.

[35] Lee A. Sotorasib: a review in KRAS G12C mutation-positive non-small cell lung cancer. Target Oncol 2022; 17: 727-733.

[36] Gao S, Zhang X, Gao K, Zhang Z, Huang Y, Yoda R and Yao J. The pivotal role of extracellular signal-regulated kinase in gap junction-mediated regulation of TXNIP. Cell Signal 2017; 38: 116-126.

[37] Akhave NS, Biter AB and Hong DS. Mechanisms of resistance to KRAS (G12C)-targeted therapy. Cancer Discov 2021; 11: 1345-1352.

[38] Zhao Y, Murciano-Goroff YR, Xue JY, Ang A, Lucas J, Mai TT, Da Cruz Paula AF, Saiki AY, Mohn D, Achanta P, Sisk AE, Arora KS, Roy RS, Kim D, Li C, Lim LP, Li M, Bahr A, Loomis BR, de Stanchina E, Reis-Filho JS, Weigelt B, Berger M, Riely G, Arbour KC, Lipford JR, Li BT and Lito P. Diverse alterations associated with resistance to KRAS (G12C) inhibition. Nature 2021; 599: 679-683.

[39] Chan CH, Chiou LW, Lee TY, Liu YR, Hsieh TH, Yang CY and Jeng YM. PAK and PI3K pathway activation confers resistance to KRAS (G12C) inhibitor sotorasib. Br J Cancer 2023; 128: 148-159.

[40] Yaeger R and Solit DB. Overcoming adaptive resistance to KRAS inhibitors through vertical pathway targeting. Clin Cancer Res 2020; 26: 1538-1540.

The effect of Sotorasib on bladder cancer

Supplementary Table 1. Chemicals and primary antibodies used in this study

Name	Supplier	Cat no.
Sotorasib	MCE	2296729-00-3
CHX	Selleck	S7418
MG132	Selleck	S2619
CQ	MedChemExpress	HY-17589AS
Selumetinib	MedChemExpress	HY-50706
TBHQ	MCE	1948-33-0
KRAS	Abcam	275876
cRAF	SAB	35408
p-c-RAF	Cell Signaling Technology	9421
p-ERK	Cell Signaling Technology	4370
ERK	Cell Signaling Technology	9102
p-AKT	Cell Signaling Technology	4060
AKT	Cell Signaling Technology	9272
p-mTOR	Cell Signaling Technology	5536
mTOR	Proteintech	20657
GLUT1	Santa	377228
PKM2	Cell Signaling Technology	4053
LDHA	Santa	137243
TXNIP	Cell Signaling Technology	14715
β-actin	SAB	52901
Ubiquitin	R&D Systems	MAB701

Supplementary Table 2. Primers used in this study

Gene	Forward Primer	Reverse Primer
SLC2A1	GTCTGGCATCAACGCTGTCT	AACAGCGACACGACAGTGAA
PKM2	CATGCAGCACCTGATAGCTC	CTTGAGGCTCGCACAAGTTC
LDHA	AGGAACAGTGGAAAGAGTGCAG	ACATGCACAACCTCCACCTA
TXNIP	TGACCTGCCCCTGGTAATTG	ATGCAGGGATCCACCTCAGTA
ACTB	CACCATTGGCAATGAGCGGTTC	AGGTCTTTGCGGATGTCCACGT

Supplementary Table 3. The targeting oligos of TXNIP

siRNA	5'-3'
genOFFTM st-h-TXNIP_001	CAACATCCTTCGAGTTGAA
si-h-TXNIP_005	TGATCATGAGACCTGGAAA